CLNS 07/2007
CLEO 07-12

# First Observation of Exclusive $\chi_{cJ}$ Decays to Two Charged and Two Neutral Hadrons


Q. He,[1] J. Insler,[1] H. Muramatsu,[1] C. S. Park,[1] E. H. Thorndike,[1] F. Yang,[1] M. Artuso,[2] S. Blusk,[2] S. Khalil,[2] J. Li,[2] N. Menaa,[2] R. Mountain,[2] S. Nisar,[2] K. Randrianarivony,[2] R. Sia,[2] N. Sultana,[2] T. Skwarnicki,[2] S. Stone,[2] J. C. Wang,[2] L. M. Zhang,[2] G. Bonvicini,[3] D. Cinabro,[3] M. Dubrovin,[3] A. Lincoln,[3] D. M. Asner,[4] K. W. Edwards,[4] P. Naik,[4] R. A. Briere,[5] T. Ferguson,[5] G. Tatishvili,[5] H. Vogel,[5] M. E. Watkins,[5] J. L. Rosner,[6] N. E. Adam,[7] J. P. Alexander,[7] D. G. Cassel,[7] J. E. Duboscq,[7] R. Ehrlich,[7] L. Fields,[7] L. Gibbons,[7] R. Gray,[7] S. W. Gray,[7] D. L. Hartill,[7] B. K. Heltsley,[7] D. Hertz,[7] C. D. Jones,[7] J. Kandaswamy,[7] D. L. Kreinick,[7] V. E. Kuznetsov,[7] H. Mahlke-Krüger,[7] D. Mohapatra,[7] P. U. E. Onyisi,[7] J. R. Patterson,[7] D. Peterson,[7] D. Riley,[7] A. Ryd,[7] A. J. Sadoff,[7] X. Shi,[7] S. Stroiney,[7] W. M. Sun,[7] T. Wilksen,[7] S. B. Athar,[8] R. Patel,[8] J. Yelton,[8] P. Rubin,[9] B. I. Eisenstein,[10] I. Karliner,[10] S. Mehrabyan,[10] N. Lowrey,[10] M. Selen,[10] E. J. White,[10] J. Wiss,[10] R. E. Mitchell,[11] M. R. Shepherd,[11] D. Besson,[12] T. K. Pedlar,[13] D. Cronin-Hennessy,[14] K. Y. Gao,[14] J. Hietala,[14] Y. Kubota,[14] T. Klein,[14] B. W. Lang,[14] R. Poling,[14] A. W. Scott,[14] P. Zweber,[14] S. Dobbs,[15] Z. Metreveli,[15] K. K. Seth,[15] A. Tomaradze,[15] K. M. Ecklund,[16] W. Love,[17] V. Savinov,[17] A. Lopez,[18] H. Mendez,[18] J. Ramirez,[18] J. Y. Ge,[19] D. H. Miller,[19] B. Sanghi,[19] I. P. J. Shipsey,[19] B. Xin,[19] G. S. Adams,[20] M. Anderson,[20] J. P. Cummings,[20] I. Danko,[20] D. Hu,[20] B. Moziak,[20] and J. Napolitano[20]

(CLEO Collaboration)

*[1]University of Rochester, Rochester, New York 14627, USA*
*[2]Syracuse University, Syracuse, New York 13244, USA*
*[3]Wayne State University, Detroit, Michigan 48202, USA*
*[4]Carleton University, Ottawa, Ontario, Canada K1S 5B6*
*[5]Carnegie Mellon University, Pittsburgh, Pennsylvania 15213, USA*
*[6]Enrico Fermi Institute, University of Chicago, Chicago, Illinois 60637, USA*
*[7]Cornell University, Ithaca, New York 14853, USA*
*[8]University of Florida, Gainesville, Florida 32611, USA*
*[9]George Mason University, Fairfax, Virginia 22030, USA*
*[10]University of Illinois, Urbana-Champaign, Illinois 61801, USA*
*[11]Indiana University, Bloomington, Indiana 47405, USA*
*[12]University of Kansas, Lawrence, Kansas 66045, USA*
*[13]Luther College, Decorah, Iowa 52101, USA*
*[14]University of Minnesota, Minneapolis, Minnesota 55455, USA*
*[15]Northwestern University, Evanston, Illinois 60208, USA*
*[16]State University of New York at Buffalo, Buffalo, New York 14260, USA*
*[17]University of Pittsburgh, Pittsburgh, Pennsylvania 15260, USA*
*[18]University of Puerto Rico, Mayaguez, Puerto Rico 00681*
*[19]Purdue University, West Lafayette, Indiana 47907, USA*
*[20]Rensselaer Polytechnic Institute, Troy, New York 12180, USA*



(Dated: June 6, 2008)

## Abstract

We study exclusive $\chi_{c0,1,2}$ decays to four-hadron final states involving two charged and two neutral mesons: $\pi^+\pi^-\pi^0\pi^0$, $K^+K^-\pi^0\pi^0$, $p\bar{p}\pi^0\pi^0$, $K^+K^-\eta\pi^0$, and $K^\pm\pi^\mp K^0\pi^0$. The $\chi_c$ states are produced in radiative decays of 3.08 million $\psi(2S)$ resonance decays and observed in the CLEO detector. We also measure the largest substructure contributions to the modes $\pi^+\pi^-\pi^0\pi^0$ and $K^\pm\pi^\mp K^0\pi^0$.

Exclusive charmonium decays have been a subject of interest for decades as they are an excellent laboratory for studying quark-gluon dynamics at relatively low energies. However, current measurements in the $P$-wave $\chi_c$ sector are sparse [1]. Although these states are not directly produced in $e^+e^-$ collisions, they are copiously produced in the radiative decays $\psi(2S) \to \gamma\chi_c$, each of which has a branching ratio of around 9% [2]. Recent data taken by the CLEO detector at the Cornell Electron Storage Ring to study $e^+e^-$ annihilations with a center of mass energy corresponding to the $\psi(2S)$ mass allow for a detailed study of $\chi_c$ decays.

Past research indicates that the Color Octet Mechanism (COM) plays a role in the decay of these $P$-wave charmonia states [3–7]. In order to build a comprehensive understanding about the $P$-wave dynamics, both theoretical predictions employing the COM and new precise experimental measurements for $\chi_c$ many-body final states are required. Furthermore, decays of $\chi_c$, in particular $\chi_{c0,2}$, may provide a window on glueball dynamics [8].

This analysis follows the general method of our earlier work on $\eta, \eta'$ [9] and three-body [10] decays of $\chi_c$, extending it to higher multiplicity states. The four-body exclusive $\chi_c$ decay modes studied in this article contain two neutral and two charged hadrons in the final state and are being measured for the first time. We also take a first look at the gross features of the rich substructure in these decay modes.

The data used in this analysis consist of 2.74 pb$^{-1}$ and 2.89 pb$^{-1}$, a total of (3.08±0.09) $\times 10^6$ $\psi(2S)$ decays, taken with the CLEO III [11] and CLEO-c [12] detector configurations, respectively. Both detector configurations provide 93% solid angle coverage, and have common components of particle identification which are critical to this analysis: the main drift chamber, the Ring Imaging Cherenkov Detector (RICH), and the CsI calorimeter (CC). We distinguish two regions of the CC in polar angle: the barrel ($|\cos(\theta)| < 0.81$) and the endcap ($|\cos(\theta)| \geq 0.81$). The CC detects photons with an energy resolution of 2.2% (5%) for photons with energy of 1 GeV (100 MeV), making it possible to resolve the three $\chi_c$ states.

The event reconstruction and final state selection criteria proceed along the lines of our recent analyses on this subject [9, 10]. We reconstruct the following $\chi_c$ decay modes: $K^+K^-\eta\pi^0$; $K^\pm\pi^\mp K^0_S\pi^0$; and $h^+h^-\pi^0\pi^0$, where $h = \pi, K, p$. In addition, we reconstruct the transition photon from $\psi(2S)$, thus detecting the entire event.

Each charged particle in the event is required to pass standard criteria for track quality and geometric acceptance. We also require the number of such tracks to be either two or four depending on the final state. We demand all tracks come from the beam spot with a momentum-dependent cut on the impact parameter. This cut is less restrictive for low-momentum tracks, for which the resolution is poorer. We combine ionization loss in the drift chamber ($dE/dx$) and RICH information to discriminate between $p, K,$ and $\pi$ using $\chi^2$ criteria discussed elsewhere [13]. Additional requirements suppress charged lepton QED backgrounds. We reject electron candidates as follows: for all tracks, we compute the ratio of CC energy to track momentum, $E_{\mathrm{CC}}/p$, and the difference between the measured $dE/dx$ and the expected $dE/dx$ for the electron hypothesis, normalized to its standard deviation, $\sigma_e$. We reject tracks with both $0.92 < E_{\mathrm{CC}}/p < 1.05$ and $|\sigma_e| < 3$. Particles that penetrate more than five nuclear interaction lengths of the muon detectors are rejected. The particle identification together with the lepton veto criteria are found to be more than 97% efficient for all the modes.

We define photon showers as those having a lateral profile in the CC consistent with a photon and possessing at least 30 MeV of energy. We require photon candidates found in the endcap CC region that are used in $\pi^0$ and $\eta$ reconstruction to possess more than

50 MeV of energy. We reconstruct $\pi^0 \to \gamma\gamma$ and $\eta \to \gamma\gamma$ candidates using a pair of photons that are kinematically fit to the nominal $\pi^0$ or $\eta$ mass using the event's charged tracks to define the origin of the photon trajectories. A cut is placed on the mass fit of $\chi^2 < 10$ (for one degree of freedom). Each $\pi^0$ and $\eta$ photon daughter is forbidden to be part of any other final state particle. We also reconstruct $\eta \to \pi^+\pi^-\pi^0$ decay by combining a pair of charged pion candidates with a $\pi^0$ and doing a mass-constrained fit to the nominal $\eta$ mass with the requirement $\chi^2 < 10$ for one degree of freedom. We reconstruct the $K^0_S$ by constraining a pair of oppositely charged pions to come from a common vertex. We require that the reconstructed invariant mass of the two pions be within 10 MeV ($\approx 3.2$ standard deviations) of the nominal $K^0_S$ mass.

We combine any unused photon with the four hadrons to reconstruct the complete event which we then constrain to the four-momentum of the $\psi(2S)$, using the nominal mass of the $\psi(2S)$ and taking into account the crossing angle between the $e^+$ and $e^-$ beams ($\approx 4$ mrad). We demand $\chi^2 < 25$ (for four degrees of freedom) for this constraint. This requirement strongly rejects background, and the fitting procedure greatly improves the mass resolution of the $\chi_c$. In $\leq 10\%$ of the events (the $\gamma\pi^+\pi^-\pi^0\pi^0$ state is worst), multiple possible pairings of photons lead to multiple $\chi_c$ candidates. We choose the one with the smallest $\chi^2$.

We study the efficiencies and resolutions of the final states by generating signal events using a GEANT-based [14] detector simulation. Over 0.7 million events were generated for the two detector configurations, three $\chi_c$ mesons, and five final states. Events were generated in accordance with an electric dipole (E1) transition production cross section of $1 + \lambda\cos^2\theta$, where $\theta$ is the radiated photon angle relative to the positron beam direction, and $\lambda = 1, -1/3, +1/13$ for $J = 0, 1, 2$ particles, respectively.

The efficiencies averaged over the CLEO III and CLEO-c datasets (weighted by the number of $\psi(2S)$ events) are listed in Table I for each final state. The efficiency includes the $\eta \to \gamma\gamma$ , $\eta \to \pi^+\pi^-\pi^0$ and $K^0_S \to \pi^+\pi^-$ branching ratios [1]. The invariant mass distributions of the final state hadrons were fitted to three signal shape functions corresponding to each of the three $\chi_c$ states and an additional constant background function. Each signal shape function consisted of a Breit-Wigner convolved with a double Gaussian resolution function. The widths of the Breit-Wigner functions are fixed to the intrinsic widths of the $\chi_c$ states: $\Gamma_{\chi_{c0}} = 10.4$ MeV, $\Gamma_{\chi_{c1}} = 0.89$ MeV, and $\Gamma_{\chi_{c2}} = 2.06$ MeV [1]. The detector resolution is obtained from simulation by a fit to the difference between the generated and reconstructed invariant mass of the $\chi_c$ products, mode-wise and separately for each $\chi_c$. The detector resolution, ranging from 4.5 to 7.1 MeV for the various final states, is less than the natural width of the $\chi_{c0}$, but greater than the natural width of the $\chi_{c1}$ and $\chi_{c2}$. The $\chi_c$ masses are fixed to their nominal values [1] during the fitting. In all cases, the reconstructed masses, when allowed to float, are consistent with the expected values.

Clean signals of $\chi_{c0}$, $\chi_{c1}$ and $\chi_{c2}$ are found in most of the modes studied as seen in Figure 1. The signal yields and efficiencies, $\varepsilon$, are listed in Table I for each final state, calculated assuming four-body phase space. The errors on the efficiencies due to limited simulation statistics are considered with other systematic uncertainties listed in Table III. The yields and efficiencies in Table I are used to calculate the final branching fractions for all modes, except $\pi^+\pi^-\pi^0\pi^0$ and $K^+\pi^-K^0\pi^0$, which we proceed to study in more detail.

We can further investigate how the decays proceed by searching for substructure in the four-hadron final states. Substructure can also affect the detection efficiency. Here we restrict ourselves to looking for the gross features of substructure by plotting the invariant mass of di-hadron combinations in the $\chi_c$ signal regions, after subtracting the yields from $\chi_c$

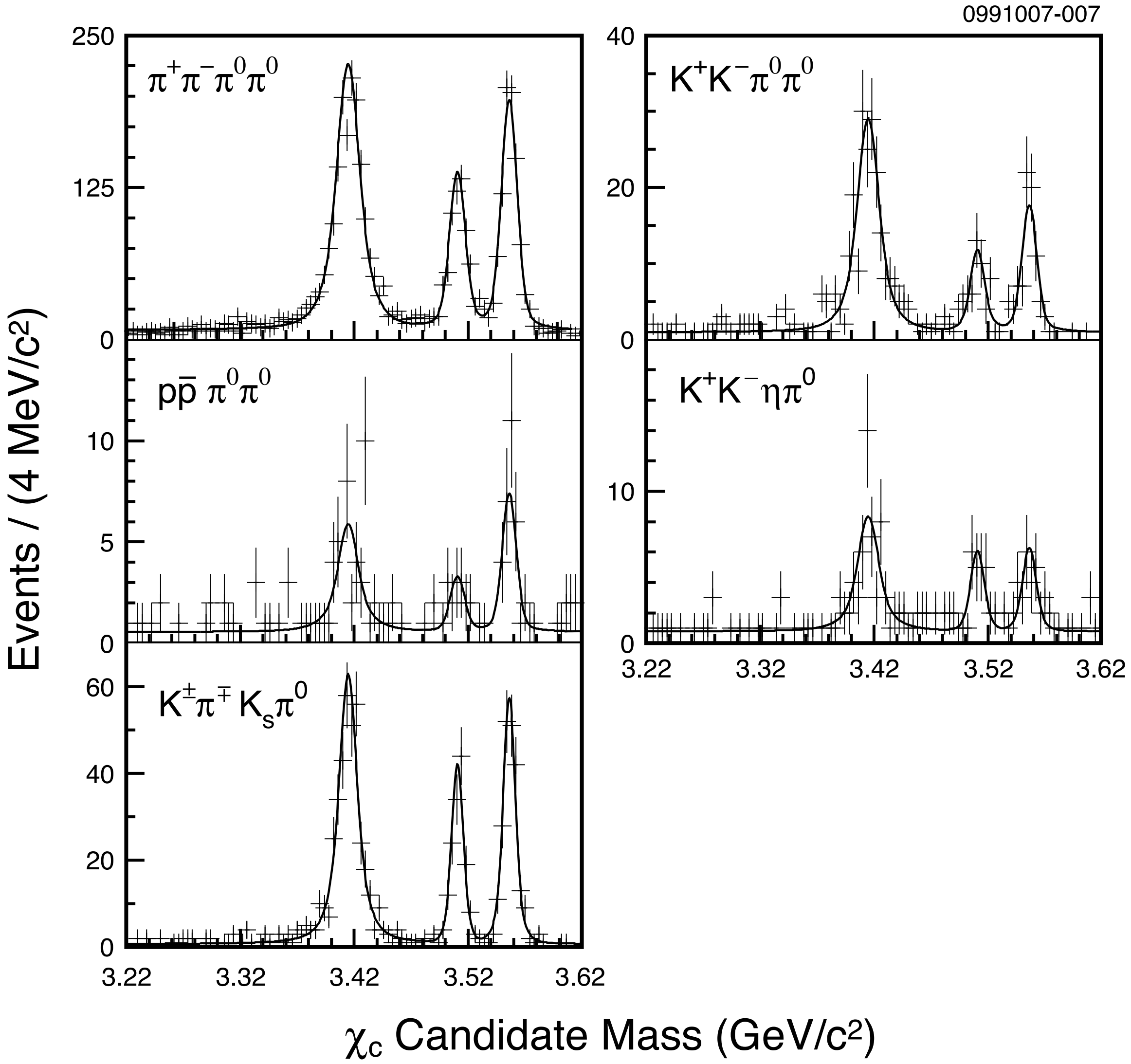


FIG. 1: The fitted distributions of the invariant mass of $\chi_c$ candidates in data. The fitting procedure is described in the text.

sidebands. The signal regions for the invariant mass distributions of $\chi_{c0}$, $\chi_{c1}$, and $\chi_{c2}$ candidates, are 3.370-3.470 GeV/$c^2$, 3.490-3.535 GeV/$c^2$ and 3.535-3.590 GeV/$c^2$, respectively. One-sided invariant mass distribution sidebands of 3.300-3.360 GeV/$c^2$, 3.470-3.490 GeV/$c^2$ and 3.590-3.625 GeV/$c^2$, respectively, are subtracted. We claim and show signals only for those cases where we observe a signal for resonant substructure with significance of $\geq 4\ \sigma$; these are all in the four body-modes $\pi^+\pi^-\pi^0\pi^0$ and $K^\pm\pi^\mp K^0\pi^0$. After identifying the intermediate states, we fit the distributions with Breit-Wigner functions for each of these intermediate states using a fixed mass and width as listed in [1], and add an additional third order polynomial function to describe the background. We obtain the efficiencies for detecting the intermediate states, $\varepsilon'$, by fitting the resonant signals using the procedure described above, in samples of events that simulated the decay as proceeding entirely through the respective intermediate states. Figures 2 and 3 show two-body intermediate states in $\pi^+\pi^-\pi^0\pi^0$ and $K^\pm\pi^\mp K^0_S\pi^0$ final states, respectively, for each of the $\chi_c$ states. In the former case there are two combinations entering the plot for each $\chi_c$ candidate. We find clear

TABLE I: Yields ($N$) and efficiencies $\varepsilon$ for four-hadron final states. Efficiencies were estimated using a Monte Carlo sample generated according to four-body phase space as described in the text.

| Mode | $\chi_{c0}$ | | $\chi_{c1}$ | | $\chi_{c2}$ | |
|---|---|---|---|---|---|---|
| | $N$ | $\varepsilon(\%)$ | $N$ | $\varepsilon(\%)$ | $N$ | $\varepsilon(\%)$ |
| $\pi^+\pi^-\pi^0\pi^0$ | 1751.4±51.3 | 17.6 | 604.7±28.5 | 17.5 | 903.5±32.6 | 17.6 |
| $K^+K^-\pi^0\pi^0$ | 213.5±16.8 | 12.7 | 45.1±8.5 | 13.1 | 76.9±9.7 | 12.6 |
| $p\bar{p}\pi^0\pi^0$ | 39.5±8.5 | 12.8 | 11.5±4.2 | 13.9 | 29.2±5.9 | 13.3 |
| $K^+K^-\eta\pi^0$ | 56.4±9.2 | 6.19 | 21.0±5.7 | 6.17 | 22.9±6.1 | 6.07 |
| $K^\pm\pi^\mp K^0_S\pi^0$ | 401.7±22.4 | 10.3 | 141.3±13.3 | 11.2 | 211.6±15.4 | 10.3 |

signals for the $\rho$ and $K^*$ mesons. The yields and efficiencies, $\varepsilon'$, of final states including these resonances are listed in Table II and are used as inputs to the final branching fraction calculations.

Several sources of systematic uncertainty in the branching fractions are listed in Table III. These include uncertainties in the number of $\psi(2S)$ particles, determined according to the method described in [2], tracking and particle identification efficiencies associated with charged particles, reconstruction efficiencies due to simulation statistics, and trigger simulation. By comparing the effect of varying the requirement on the $\chi^2$ of the constrained four-momentum fit in data and in simulated events, we estimate a ±4.0% systematic error in modelling the $\chi^2$ distribution. The uncertainty in the efficiency of the transition photon reconstruction for each of the final states is taken to be 2%. In addition, the systematic uncertainties for $\pi^0$ and $\eta$ efficiencies are 4% for each $\pi^0$ or $\eta$ meson in the final state. $K^0_S$ reconstruction introduces an additional uncertainty of 2% in one of the modes. The robustness of the fitting procedure was checked by systematically re-fitting the $\chi_c$ invariant mass plots using 1 $\sigma$ variations of masses, widths, and resolutions. The uncertainties estimated from this study vary between 0.2% and 0.7%. To account for the systematic error arising from deviations in the angular distributions of final states due to the presence of intermediate resonances, a sample of events that simulated the decay as proceeding through the respective intermediate states, was generated for the substructure modes: $f_0(980)\pi^0\pi^0$, $f_2(1270)\pi^0\pi^0$, $\rho^\pm\pi^\mp\pi^0$ and $f_0(980)\pi^+\pi^-$ for the non-resonant mode $\pi^+\pi^-\pi^0\pi^0$; $K^{*\pm}K^\mp\pi^0$ and $f_0(980)K^+K^-$ for the non-resonant mode $K^+K^-\pi^0\pi^0$; $K^{*0}K^0_S\pi^0$, $K^{*\pm}K^0_S\pi^\mp$, $K^{*\pm}K^\mp\pi^0$, $\rho^\pm K^\mp K^0_S$, $K^{*0}K^\pm\pi^\mp$ and $K_1(1270)K^0_S$ for the non-resonant mode $K^\pm\pi^\mp K^0_S\pi^0$. We obtained the efficiencies of both the resonant and non-resonant modes by fitting the $\chi_c$ signals obtained from MC events with and without substructure. Based on the differences in efficiencies between final states with and without intermediate resonances, and assuming that there can be no additional unobserved resonances that can be more than 50% of the signal, we estimate the systematic error to be between 3.5% and 7.4% for the modes we studied. For the remaining modes, we conservatively assign a 7.5% systematic error based on an assumption that up to 75% of our events may contain substructure, and that the difference in efficiency of these resonant events to the non-resonant is no more than 10%.

Systematic uncertainties for the intermediate state resonance modes include common sources to their non-resonant final states. Uncertainties were added in quadrature, and those due to the branching fractions of $\psi(2S) \to \gamma\chi_c$ [2] are quoted separately. We use the values of $\mathcal{B}(\psi(2S) \to \gamma\chi_c)$ in [2], as those measurements use a subset of our data and similar analysis criteria, thereby enhancing the cancellation of systematic errors. For all final states

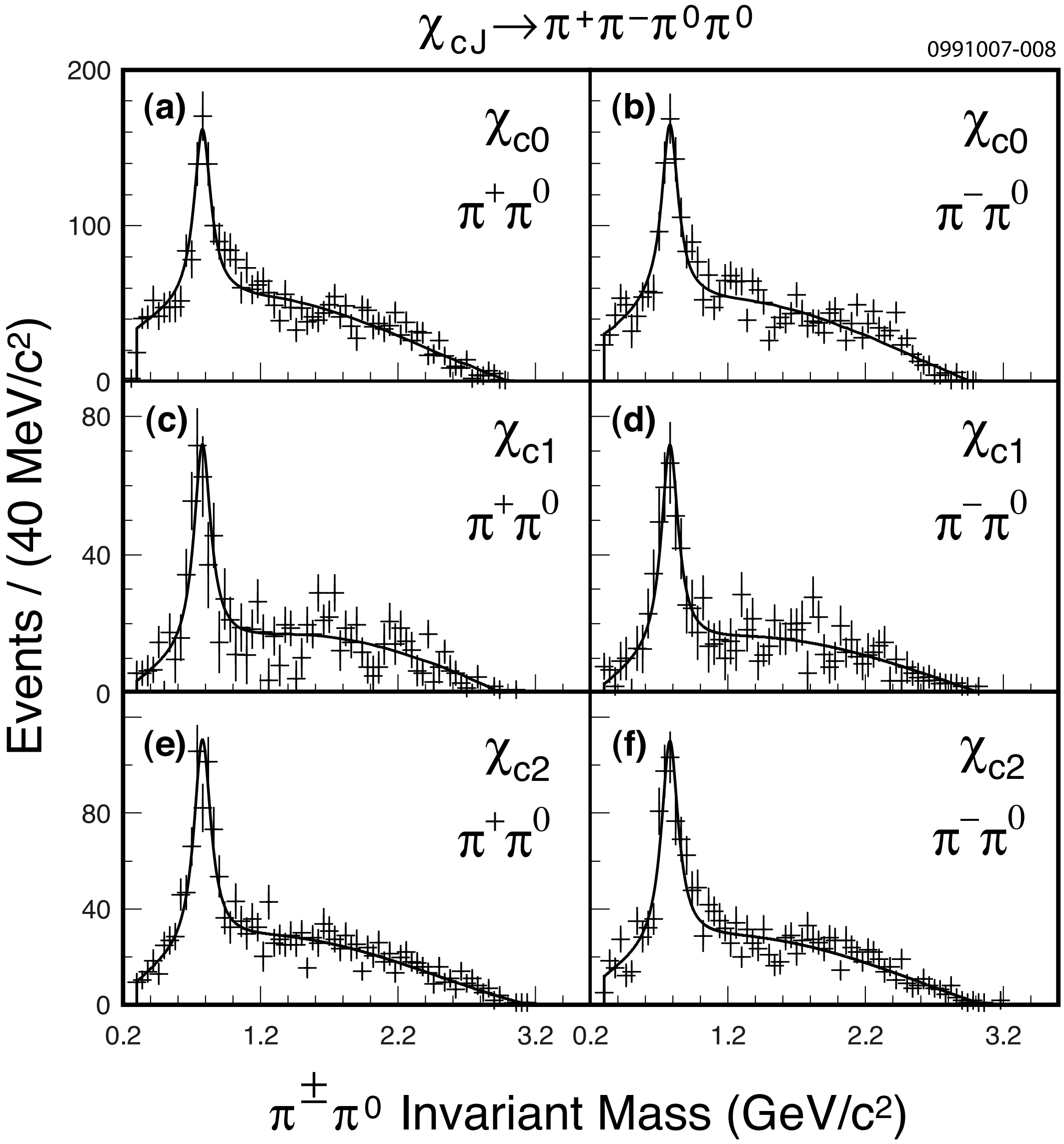


FIG. 2: Intermediate states for the decay $\chi_{cJ} \to \pi^+\pi^-\pi^0\pi^0$. Invariant mass combinations of (a) $\pi^+\pi^0$ for $J = 0$, (b) $\pi^-\pi^0$ for $J = 0$, (c) $\pi^+\pi^0$ for $J = 1$, (d) $\pi^-\pi^0$ for $J = 1$, (e) $\pi^+\pi^0$ for $J = 2$, and (f) $\pi^-\pi^0$ for $J = 2$ are shown after sideband subtraction. All plots show significant evidence for production of $\rho^\pm$.

except $\pi^+\pi^-\pi^0\pi^0$ and $K^\pm\pi^\mp K_s\pi^0$, we convert the yields in Tables I and II to branching fractions using:

$$\mathcal{B}(\chi_{cJ} \to i) = \frac{N_i}{N_{\psi(2S)} \cdot \varepsilon_i \cdot \mathcal{B}(\psi(2S) \to \gamma\chi_{cJ})} \tag{1}$$

where $N_i$ is the yield; $N_{\psi(2S)}$ is the number of $\psi(2S) = 3.08 \times 10^6$; $\varepsilon$ is the same $\varepsilon$ listed in Table I for four-hadron modes, or $\varepsilon'$ listed in Table II for substructure modes, and $i$ represents a particular decay mode.

To calculate the branching fractions for the inclusive four-hadron final states for $\pi^+\pi^-\pi^0\pi^0$ and $K^\pm\pi^\mp K^0\pi^0$ we use a modified procedure. Since the $\rho^\pm\pi^\mp\pi^0$ clearly domi-

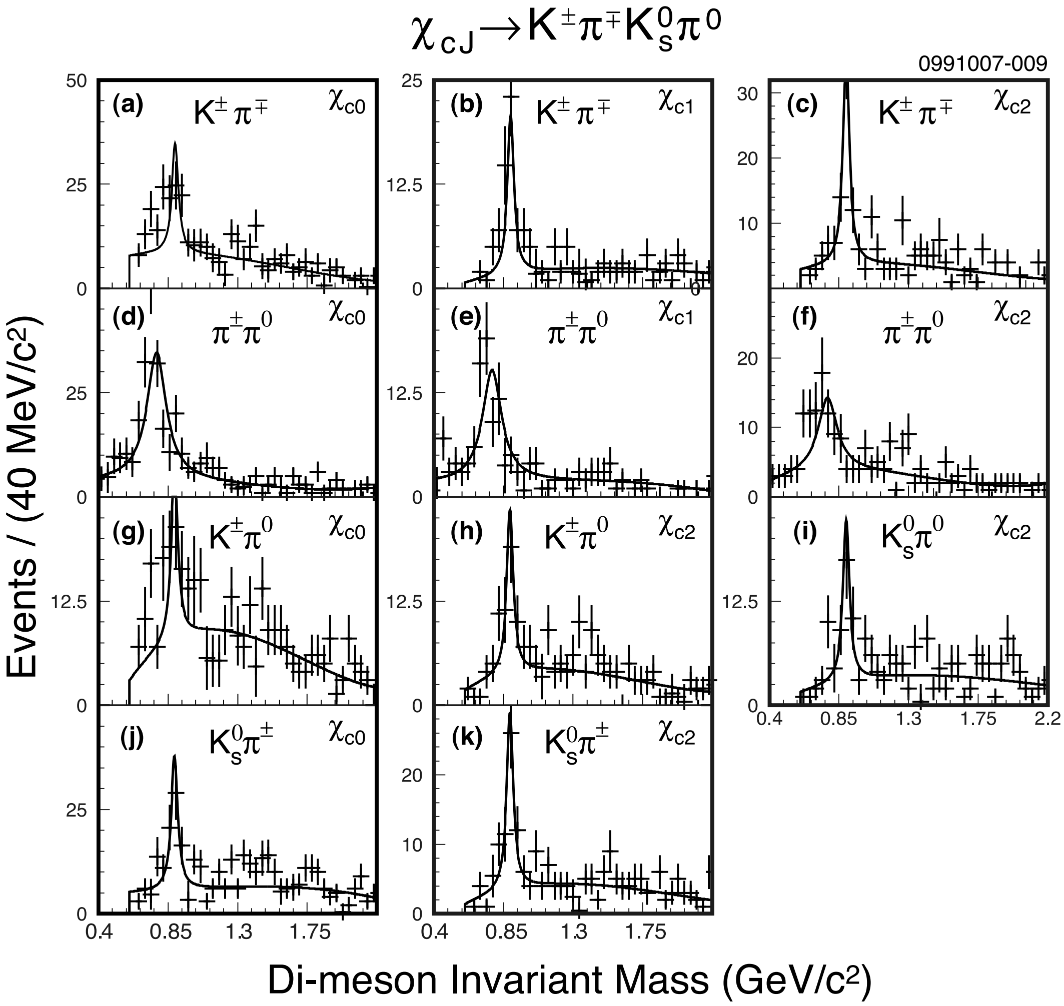


FIG. 3: Figure shows intermediate states for the decay $\chi_{cJ} \to K^\pm\pi^\mp K^0_S\pi^0$. Invariant mass combinations of (a) $K^\pm\pi^\mp$ for $J=0$, (b) $K^\pm\pi^\mp$ for $J=1$, (c) $K^\pm\pi^\mp$ for $J=2$, (d) $\pi^\pm\pi^0$ for $J=0$, (e) $\pi^\pm\pi^0$ for $J=1$, (f) $\pi^\pm\pi^0$ for $J=2$, (g) $K^\pm\pi^0$ for $J=0$, (h) $K^\pm\pi^0$ for $J=2$, (i) $K^0_S\pi^0$ for $J=2$ (j) $\pi^\pm K^0_S$ for $J=0$, and (k) $\pi^\pm K^0_S$ for $J=2$ are shown after sideband subtraction. Strong signals for $\rho^\pm$ or $K^*$ production are visible.

nates the four-hadron final state yields for the $\pi^+\pi^-\pi^0\pi^0$ mode (Tables I and II), we use the efficiency $\varepsilon$ of the $\rho^\pm\pi^\mp\pi^0$ sub-mode listed in Table II and Equation 1 to determine the $\pi^+\pi^-\pi^0\pi^0$ branching fraction. The efficiencies $\varepsilon$ were obtained by fitting the $\chi_{cJ}$ signals in substructure simulations using the same fitting procedure as that used for the four-hadron signal simulations[1]. To calculate the $K^\pm\pi^\mp K^0\pi^0$ branching fraction, we modify the procedure by taking into account that this channel has many intermediate resonances (Table II). We replace the ratio $N_i/e_i$ in Equation 1 with an efficiency corrected yield ($Y_{K^\pm\pi^\mp K^0\pi^0}$) by adding the individual efficiency corrected contributions of all resonant and non-resonant

[1] The efficiency $\varepsilon'$ is lower than $\varepsilon$ since the sideband subtraction procedure used for obtaining the efficiency $\varepsilon'$ results in some loss of efficiency.

TABLE II: Yields and efficiencies (in %) for substructure modes. $\varepsilon$ represents the efficiency obtained by fitting the $\chi_c$ signals using the same procedure as that used for the non-resonant four-hadron modes, in substructure simulated samples. Efficiency $\varepsilon'$ was obtained by fitting the intermediate peaks after applying the sideband subtraction procedure described in the text. $N'$ describes the yield corresponding to this efficiency $\varepsilon'$.

| Mode | $\chi_{c0}$ | | | $\chi_{c1}$ | | | $\chi_{c2}$ | | |
|---|---|---|---|---|---|---|---|---|---|
| | $N'$ | $\varepsilon$ | $\varepsilon'$ | $N'$ | $\varepsilon$ | $\varepsilon'$ | $N'$ | $\varepsilon$ | $\varepsilon'$ |
| $\rho^+\pi^-\pi^0$ | 661.4±56.8 | 17.4 | 15.7 | 355.7±42.1 | 16.9 | 16.3 | 519.3±38.7 | 16.8 | 16.1 |
| $\rho^-\pi^+\pi^0$ | 697.1±56.6 | 17.4 | 15.7 | 356.6±41.0 | 16.9 | 16.3 | 512.6±40.0 | 16.8 | 16.1 |
| $K^{*0}K^0_S\pi^0$, $K^{*0}\to K^\pm\pi^\mp$ | 52.5±12.1 | 11.0 | 9.94 | 37.9±8.5 | 11.1 | 10.9 | 63.0±10.5 | 11.5 | 11.2 |
| $K^{*0}K^\pm\pi^\mp$, $K^{*0}\to K^0_S\pi^0$ | - | | | - | | | 38.7±9.0 | 9.50 | 9.14 |
| $K^{*\pm}K^\mp\pi^0$, $K^{*\pm}\to\pi^\pm K^0_S$ | 64.1±12.8 | 10.3 | 9.30 | - | | | 51.1±9.8 | 9.66 | 9.40 |
| $K^{*\pm}\pi^\mp K^0_S$, $K^{*\pm}\to K^\pm\pi^0$ | 42.5±10.0 | 10.4 | 9.44 | - | | | 39.3±8.7 | 9.44 | 9.10 |
| $\rho^\pm K^\mp K^0_S$ | 179.7±22.7 | 11.0 | 9.92 | 79.5±16.9 | 10.8 | 10.6 | 62.9±15.9 | 10.8 | 10.5 |

TABLE III: Systematic uncertainties (fractional errors in %). The overall systematic uncertainty is obtained by adding the individual contributions in quadrature, with the exception of the photon simulation uncertainty which adds linearly with the $\pi^0$ and $\eta$ reconstruction uncertainties.

| Source | $\pi^+\pi^-\pi^0\pi^0$ | $K^+K^-\pi^0\pi^0$ | $p\bar{p}\pi^0\pi^0$ | $K^+K^-\eta\pi^0$ | $K^\pm\pi^\mp K^0_S\pi^0$ |
|---|---|---|---|---|---|
| $N_{\psi(2S)}$ | 3.0 | 3.0 | 3.0 | 3.0 | 3.0 |
| Tracking efficiency | 1.4 | 1.4 | 1.4 | 1.4 | 2.8 |
| Particle identification | 0.6 | 2.6 | 2.6 | 2.6 | 2.2 |
| Simulation statistics | 1.9 | 2.3 | 2.3 | 2.8 | 4.5 |
| Trigger efficiency | 1.0 | 1.0 | 1.0 | 1.0 | 1.0 |
| Kinematic constraint cut | 4.0 | 4.0 | 4.0 | 4.0 | 4.0 |
| Transition $\gamma$ simulation | 2.0 | 2.0 | 2.0 | 2.0 | 2.0 |
| $\pi^0,\eta\to\gamma\gamma$ reconstruction | 8.0 | 8.0 | 8.0 | 8.0 | 4.0 |
| $K^0_S$ Vertexing | 0.0 | 0.0 | 0.0 | 0.0 | 2.0 |
| Fitting procedure | 0.5 | 0.6 | 0.7 | 0.7 | 0.2 |
| Model dependence | 3.5 | 7.4 | 7.5 | 7.5 | 6.0 |
| **Overall** | **12.0** | **14.0** | **14.0** | **14.1** | **11.6** |

channels computed as:

$$Y_{K^\pm\pi^\mp K^0\pi^0} = \frac{N_{K^\pm\pi^\mp K^0\pi^0}}{\varepsilon_{K^\pm\pi^\mp K^0\pi^0}} + \sum_{k=1}^{5} \frac{N_k}{\varepsilon'_k}\cdot\left(1-\frac{\varepsilon_k}{\varepsilon_{K^\pm\pi^\mp K^0\pi^0}}\right) \tag{2}$$

where $k$ runs over the substructure modes we consider, $K^{*0}K^0_S\pi^0$, $K^{*0}K^\pm\pi^\mp$, $K^{*\pm}K^\mp\pi^0$, $K^{*\pm}\pi^\mp K^0_S$, and $\rho^\pm K^\mp K^0_S$.

The branching fractions obtained and their uncertainties are summarized in Table IV. Where we do not find evidence of a signal, we present a 90% C.L. upper limit by determining the value that includes 90% of the probability density function (p.d.f) obtained by convolving the p.d.f for the branching fraction with a Gaussian systematic error.

The results of the branching fractions of the four-hadron modes studied in this analysis include both resonant and non-resonant contributions. Our three-hadron intermediate resonance branching fractions are inclusive and may contain additional resonant substructure that we do not explicitly measure; therefore, the branching fraction measurements cannot be trivially related to the amplitude for the specific three-body non-resonant decay. We assume variations of the efficiency due to this additional substructure produce changes in the branching fractions within the model dependence systematic error.

We compare the branching fractions $\chi_{cJ} \to \rho^{\pm}\pi^{\mp}\pi^{0}$ for $J = 0, 1, 2$ (Table IV) with measurements of $\chi_{cJ} \to \rho^{0}\pi^{+}\pi^{-}$ [1], and observe that our results are consistent with a ratio equal to unity as expected from isospin conservation.

Furthermore, we also find our measurement of $\mathcal{B}(\chi_{c2} \to K^{*0}K^{\pm}\pi^{\mp})$ (Table V) to be consistent within experimental errors with $\mathcal{B}(\chi_{c2} \to K^{*0}K^{\pm}\pi^{\mp})$ of [1]. Our results are consistent with the expected isospin-related prediction that $\chi_c \to K^{*}K\pi$ where $\chi_c \to K^{*0}K^{0}\pi^{0}$ and $\chi_c \to K^{*\pm}K^{\mp}\pi^{0}$ have equal partial widths. Moreover, our measurements for $\mathcal{B}(\chi_{c2} \to K^{*0}K^{\pm}\pi^{\mp})$, $\mathcal{B}(\chi_{c0} \to K^{*\pm}\pi^{\mp}K^{0})$, and $\mathcal{B}(\chi_{c2} \to K^{*\pm}\pi^{\mp}K^{0})$ (Table V) are in good agreement with the isospin expectation of

$$\mathcal{B}(\chi_c \to K^{*0}K^{0}\pi^{0}) : \mathcal{B}(\chi_c \to K^{*0}K^{\pm}\pi^{\mp}) = 1 : 2 \tag{3}$$

and

$$\mathcal{B}(\chi_c \to K^{*0}K^{0}\pi^{0}) : \mathcal{B}(\chi_c \to K^{*\pm}\pi^{\mp}K^{0}) = 1 : 2. \tag{4}$$

TABLE IV: Branching fractions $\mathcal{B}$ with statistical and systematic uncertainties are shown. The symbol "×" indicates product of branching fractions. The third error in each case is due to the $\psi(2S) \to \gamma\chi_c$ branching fractions. Upper limits shown are at the 90% C.L and include all the systematic errors. The first line of each set of measurements includes the contributions from the substructure listed below.

| Mode | $\chi_{c0}$ | $\chi_{c1}$ | $\chi_{c2}$ |
|---|---|---|---|
| | $\mathcal{B}$ (%) | $\mathcal{B}$ (%) | $\mathcal{B}$ (%) |
| $\pi^{+}\pi^{-}\pi^{0}\pi^{0}$ | 3.54±0.10±0.43±0.18 | 1.28±0.06±0.15±0.08 | 1.87±0.07±0.22±0.13 |
| $\rho^{+}\pi^{-}\pi^{0}$ | 1.48±0.13±0.18±0.08 | 0.78±0.09±0.09±0.05 | 1.12±0.08±0.13±0.08 |
| $\rho^{-}\pi^{+}\pi^{0}$ | 1.56±0.13±0.19±0.08 | 0.78±0.09±0.09±0.05 | 1.11±0.09±0.13±0.08 |
| $K^{+}K^{-}\pi^{0}\pi^{0}$ | 0.59±0.05±0.08±0.03 | 0.12±0.02±0.02±0.01 | 0.21±0.03±0.03±0.01 |
| $p\bar{p}\pi^{0}\pi^{0}$ | 0.11±0.02±0.02±0.01 | $< 0.05$ | 0.08±0.02±0.01±0.01 |
| $K^{+}K^{-}\eta\pi^{0}$ | 0.32±0.05±0.05±0.02 | 0.12±0.03±0.02±0.01 | 0.13±0.04±0.02±0.01 |
| $K^{\pm}\pi^{\mp}K^{0}\pi^{0}$ | 2.64±0.15±0.31±0.14 | 0.92±0.09±0.11±0.06 | 1.41±0.11±0.16±0.10 |
| $K^{*0}K^{0}\pi^{0}\times\ K^{*0} \to K^{\pm}\pi^{\mp}$ | 0.37±0.09±0.04±0.02 | 0.25±0.06±0.03±0.02 | 0.39±0.07±0.05±0.03 |
| $K^{*0}K^{\pm}\pi^{\mp}\times\ K^{*0} \to K^{0}\pi^{0}$ | - | - | 0.30±0.07±0.04±0.02 |
| $K^{*\pm}K^{\mp}\pi^{0}\times\ K^{*\pm} \to \pi^{\pm}K^{0}$ | 0.49±0.10±0.06±0.03 | - | 0.38±0.07±0.04±0.03 |
| $K^{*\pm}\pi^{\mp}K^{0}\times\ K^{*\pm} \to K^{\pm}\pi^{0}$ | 0.32±0.07±0.04±0.02 | - | 0.30±0.07±0.04±0.02 |
| $\rho^{\pm}K^{\mp}K^{0}$ | 1.28±0.16±0.15±0.07 | 0.54±0.11±0.06±0.03 | 0.42±0.11±0.05±0.03 |

In summary, the branching fractions for $\chi_{cJ} \to \pi^{+}\pi^{-}\pi^{0}\pi^{0}$, $\chi_{cJ} \to K^{+}K^{-}\pi^{0}\pi^{0}$, $\chi_{cJ} \to K^{+}K^{-}\eta\pi^{0}$, and $\chi_{cJ} \to K^{\pm}\pi^{\mp}K^{0}\pi^{0}$ for $J = 0, 1, 2$ and, $\chi_{cJ} \to p\bar{p}\pi^{0}\pi^{0}$ for $J = 0, 2$ are measured for the first time. For the mode $\chi_{c1} \to p\bar{p}\pi^{0}\pi^{0}$ upper limits at 90% C.L. are presented.

TABLE V: Branching fractions and total error measurements for the isospin-related $K^*K\pi$ intermediate modes.

| Mode | $\chi_{c0}$ | $\chi_{c1}$ | $\chi_{c2}$ |
|---|---|---|---|
| | $\mathcal{B}$ (%) | $\mathcal{B}$ (%) | $\mathcal{B}$ (%) |
| $K^{*0}K^0\pi^0$ | 0.56±0.15 | 0.38±0.11 | 0.59±0.14 |
| $K^{*0}K^\pm\pi^\mp$ | - | - | 0.90±0.25 |
| $K^{*\pm}K^\mp\pi^0$ | 0.74±0.18 | - | 0.57±0.13 |
| $K^{*\pm}\pi^\mp K^0$ | 0.96±0.25 | - | 0.90±0.25 |

We also measure for the first time the partial branching fractions of $\chi_{cJ} \to \rho^-\pi^+\pi^0$, $\chi_{cJ} \to K^{*0}K^0\pi^0$, and $\chi_{cJ} \to \rho^\pm K^\mp K^0$ for $J = 0, 1, 2$; $\chi_{c2} \to K^{*0}K^\pm\pi^\mp$; $\chi_{cJ} \to K^{*\pm}K^\mp\pi^0$and $\chi_{cJ} \to K^{*\pm}\pi^\mp K^0$ for $J = 0, 2$. These four-hadron final states account for up to 8% of the hadronic width of the $\chi_c$ states.

These measurements improve our existing knowledge of the exclusive multi-body decay modes of the $\chi_c$ states and provide insight into their decay mechanisms. The four-hadron final states $\pi^+\pi^-\pi^0\pi^0$ and $K^\pm\pi^\mp K^0\pi^0$ contain a rich substructure of intermediate resonances. These interesting results form a basis from which higher statistics studies of hadronic $\chi_c$ states and their substructure may follow.

We gratefully acknowledge the effort of the CESR staff in providing us with excellent luminosity and running conditions. D. Cronin-Hennessy and A. Ryd thank the A.P. Sloan Foundation. This work was supported by the National Science Foundation, the U.S. Department of Energy, and the Natural Sciences and Engineering Research Council of Canada.

[1] W.-M. Yao *et al.* (Particle Data Group), J. Phys. G **33**, 1 (2006).
[2] S. B. Athar *et al.* (CLEO Collaboration), Phys. Rev. D **70**, 112002 (2004).
[3] H. W. Huang and K. T. Chao, Phys. Rev. D **54**, 6850 (1996).
[4] A. Petrelli, Phys. Lett. B **380**, 159 (1996).
[5] J. Bolz, P. Kroll and G. A. Schuler, Phys. Lett. B **392**, 198 (1997).
[6] S. M. H. Wong, Nucl. Phys. A **674**, 185 (2000).
[7] S. M. H. Wong, Eur. Phys. J. C **14**, 643 (2000).
[8] C. Amsler and F. E. Close, Phys. Rev. D **53**, 295 (1996).
[9] G. S. Adams *et al.* (CLEO Collaboration), Phys. Rev. D **75**, 071101 (2007).
[10] S. B. Athar *et al.* (CLEO Collaboration), Phys. Rev. D **75**, 032002 (2007).
[11] G. Viehhauser *et al.*, Nucl. Instrum. Meth. A **462**, 146 (2001); D. Peterson *et al.*, Nucl. Instrum. Meth. Phys. Res. A **478**, 142 (2002); M. Artuso *et al.*, Nucl. Instrum. Meth. A **554**, 147 (2005).
[12] R. A. Briere *et al.* (CESR-c and CLEO-c Taskforces, CLEO-c Collaboration), Cornell University, LEPP Report No. CLNS 01/1742 (2001), unpublished.
[13] S. Dobbs *et al.* (CLEO Collaboration), Phys. Rev. D **74**, 011105 (2006).
[14] R. Brun *et al.*, Geant 3.21, CERN Program Library Long Writeup W5013 (1993), unpublished.